

From Misaligned Sub-Saturns to Aligned Brown Dwarfs: The Highest M_p/M_* Systems Exhibit Low Obliquities, Even around Hot Stars

JACE RUSZNAK,¹ XIAN-YU WANG,¹ MALENA RICE,² AND SONGHU WANG¹

¹Department of Astronomy, Indiana University, 727 East 3rd Street, Bloomington, IN 47405-7105, USA

²Department of Astronomy, Yale University, 219 Prospect St., New Haven, CT 06511, USA

ABSTRACT

We present a pattern emerging from stellar obliquity measurements in single-star systems: planets with high planet-to-star mass ratios ($M_p/M_* > 2 \times 10^{-3}$) — such as super-Jupiters, brown dwarf companions, and M-dwarfs hosting Jupiter-like planets — tend to be aligned, even around hot stars. This alignment represents a 3.7σ deviation from the obliquity distribution observed in systems with lower mass ratios ($M_p/M_* < 2 \times 10^{-3}$), which predominantly include Jupiters and sub-Saturns. The only known outlier system, XO-3, exhibits misalignment confirmed via our newly collected Rossiter-McLaughlin effect measurement ($\lambda = 41.8_{-2.0}^{+2.1}\circ$). However, the relatively large *Gaia* Renormalized Unit Weight Error (RUWE) of XO-3 suggests that it may harbor an undetected binary companion, potentially contributing to its misalignment. Given that tidal realignment mechanisms are weak for hot stars, the observed alignment in high M_p/M_* systems is likely *primordial* rather than resulting from tidal interactions. One possible explanation is that only dynamically isolated planets can continue accreting gas and evolve into super-Jupiters while maintaining their primordial alignment. Conversely, planets formed in compact configurations may be unable to grow beyond the gap-opening mass, for which our work suggests an empirical boundary $M_p/M_* = 2 \times 10^{-3}$ identified between aligned high M_p/M_* systems and misaligned low M_p/M_* systems, with dynamical instabilities contributing to the diverse spin-orbit misalignments observed in the latter.

Keywords: exoplanet dynamics (490), star-planet interactions (2177), exoplanets (498), planetary theory (1258), exoplanet systems (484)

1. INTRODUCTION

The angle between the stellar spin axis and the net orbital axis of a planetary system, known as the spin-orbit angle or stellar obliquity, serves as a valuable probe of the dynamical history of planetary systems. The near-coplanar, low-stellar-obliquity configuration of our Solar System suggests a relatively quiescent formation framework (Kant 1755; de Laplace 1796). However, this aligned configuration is not universal among exoplanetary systems: hot Jupiters exhibit a broad range of stellar spin-orbit angles (Winn et al. 2010; Schlaufman 2010; Triaud et al. 2010; Albrecht et al. 2012; Winn & Fabrycky 2015; Albrecht et al. 2022; Knudstrup et al. 2024). Specifically, previous work has shown that hot

Jupiters orbiting hot, massive stars often display significant spin-orbit misalignment, whereas those around cool, low-mass stars tend to remain aligned (Winn et al. 2010; Schlaufman 2010).

Winn et al. (2010) proposed that hot-Jupiter systems may initially be misaligned, with tidal forces realigning cool-star systems with thick convective zones, while hot-star systems with thinner convective zones remain misaligned (Albrecht et al. 2012; Xue et al. 2014; Valsecchi & Rasio 2014; Li & Winn 2016; Anderson et al. 2021; Wang et al. 2021; Rice et al. 2022a; Spalding & Winn 2022; Zanazzi et al. 2024; Zanazzi & Chiang 2024). Wu et al. (2023) suggest that, even if tidal realignment occurs, the initial obliquity distributions — prior to the potential erasure of misalignments by tidal effects — may differ between hot Jupiters orbiting cool stars and those around hot stars. High-mass stars with high-mass disks may be more likely to generate multiple Jupiters, which can induce misalignments through planet-planet inter-

Corresponding author: Jace Rusznak
 jcruszna@iu.edu

actions (Chatterjee et al. 2008; Wu & Lithwick 2013). In contrast, low-mass stars with low-mass disks may be more likely to host a single Jupiter, which undergoes quiescent dynamical evolution.

Tentative evidence for alignment in high M_p/M_* systems has been noted in previous work. Hébrard et al. (2011) first observed that massive ($\gtrsim 3 M_J$) planets lack very high obliquities ($>40^\circ$), a finding later emphasized by Triaud (2018). Zhou et al. (2019a) subsequently reported that the massive planet HATS-70 b has a low stellar obliquity, strengthening this trend. Gan et al. (2024) highlighted the alignment of TOI-4201 b, an hot Jupiter orbiting an M dwarf, further contributing to this alignment tendency. Albrecht et al. (2022) recently compiled a stellar obliquity catalog including 105 hot-Jupiter systems and found that planets with a mass ratio $M_p/M_* > 2 \times 10^{-3}$ tend to have low stellar obliquities. However, they observed that this alignment trend does not hold for very hot stars ($T_{\text{eff}} \geq 7000$ K). Hixenbaugh et al. (2023) also found suggestive evidence that systems with high M_p/M_* tend to be aligned, even around hot stars, with XO-3 being the only outlier (although it is excluded from their Figure 2 due to the y-axis cutoff).

XO-3 b is a massive hot Jupiter ($M_p = 13 M_J$) with a planet-star mass ratio of $M_p/M_* = 9 \times 10^{-3}$, orbiting a very hot star ($T_{\text{eff}} = 6,770$ K) on a 3.2-day orbit. As the first exoplanet measured to have a large spin-orbit misalignment, XO-3 b has been the subject of multiple measurements over time (Hébrard et al. (2008), $70 \pm 15^\circ$; Winn et al. (2009), $37.3 \pm 3.7^\circ$; Hirano et al. (2011a), $37.3 \pm 3.0^\circ$), which do not fully agree with each other. Although all previous datasets suffer from systematic noise (see Hirano et al. (2011a) and Worku et al. (2022) for detailed discussion), the discrepancies could also reflect true temporal variations in the spin-orbit angle (Rogers et al. 2012).

In this work, with newly collected in-transit spectroscopic observation from the NEID spectrograph, we conducted Rossiter-McLaughlin (Rossiter 1924; McLaughlin 1924) and Doppler Tomography (Albrecht et al. 2007; Collier Cameron et al. 2010) analyses to re-determine the sky-projected spin-orbit angle of XO-3 and to revisit the population-level alignment trend for systems with high M_p/M_* . This is the 14th result from the Stellar Obliquities in Long-period Exoplanet Systems (SOLES) survey (Rice et al. 2021; Wang et al. 2022; Rice et al. 2022b, 2023a; Hixenbaugh et al. 2023; Dong et al. 2023; Wright et al. 2023; Rice et al. 2023b; Lubin et al. 2023; Hu et al. 2024; Radzom et al. 2024; Ferreira dos Santos et al. 2024; Wang et al. 2024).

Our global modeling results confirm the misaligned configuration for XO-3 b, with $\lambda = 41.8^{+2.1}_{-2.0}{}^\circ$. This

result is consistent with prior high-precision measurements to within 1.3σ (Winn et al. (2009), $37.3 \pm 3.7^\circ$; Hirano et al. (2011a), $37.3 \pm 3.0^\circ$), suggesting no temporal variation in the spin-orbit angle in accordance with the conclusions of Worku et al. (2022). Furthermore, our analysis of the stellar obliquity distribution as a function of planet-star mass ratio confirms the boundary values previously reported by Hébrard et al. (2011); Triaud (2018); Zhou et al. (2019a); Albrecht et al. (2022); Hixenbaugh et al. (2023); Gan et al. (2024): systems with $M_p/M_* > 2 \times 10^{-3}$ tend to have low obliquities, even around hot stars, with a statistical significance of 3.7σ .

The structure of this paper is as follows. In Section 2, we describe the spectroscopic observations and their reduction. The derivation of atmospheric stellar parameters is outlined in Section 3. The global modeling is detailed in Section 4. A population analysis is provided in Section 5, with a summary presented in Section 6.

2. IN-TRANSIT SPECTROSCOPIC OBSERVATIONS

In-transit spectroscopic observations of XO-3 were conducted on 2021 October 27 from 4:04–10:27 UT using the NEID spectrograph (Schwab et al. 2016) on the WIYN 3.5-meter telescope at Kitt Peak National Observatory in Arizona. We adopted the high-resolution mode ($R \sim 110,000$) with an exposure time of 720 s. The observations spanned 6.3 hours, encompassing a full transit (3 hours), a 1.8-hour baseline before ingress, and a 1.5-hour baseline after egress. During the observations, atmospheric seeing ranged from $0.6''$ to $2.0''$, with a median seeing of $1.5''$, and the median airmass was 1.2.

The NEID spectra were analyzed using the NEID Data Reduction Pipeline (NEID-DRP) v1.3.0¹, which utilizes the cross-correlation function (CCF) method to derive radial velocities. The resulting signal-to-noise ratio of the barycentric-corrected radial velocities for re-weighted orders ranged from 149 to 290, with a median value of 239, leading to RV uncertainties ranging from 0.04 to 0.07 km/s.

2.1. *TESS* Photometry

In this work, we adopted the Transiting Exoplanet Survey Satellite (*TESS*; Ricker et al. 2015) Presearch Data Conditioning simple aperture photometry (PDC-SAP; Smith et al. 2012; Stumpe et al. 2012, 2014) data, which was processed by the *TESS* Science Processing

¹ <https://neid.ipac.caltech.edu/docs/NEID-DRP/>

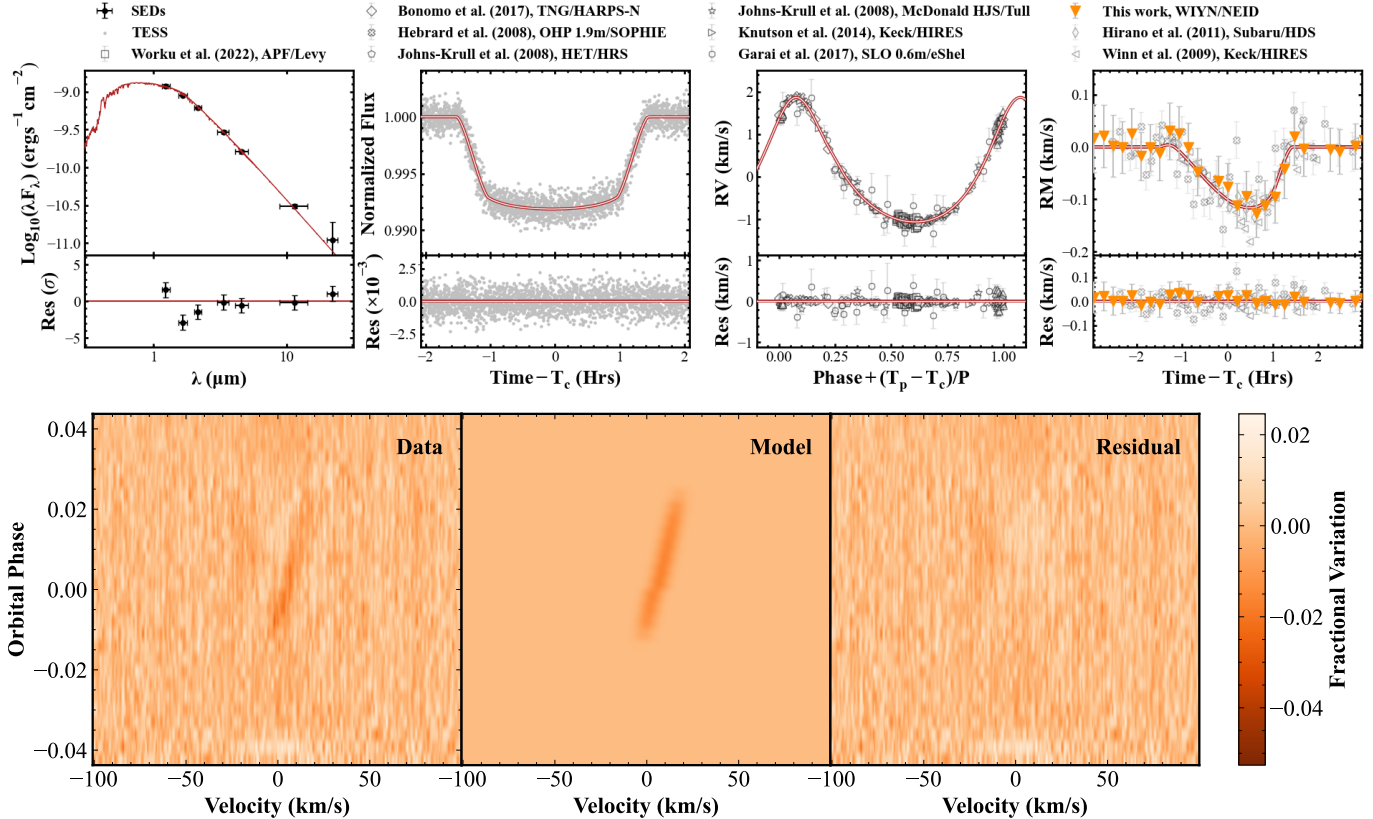


Figure 1. *Upper panel:* Spectral energy distribution, *TESS* transit photometry, out-of-transit RV, and in-transit Rossiter-McLaughlin datasets and associated best-fit EXOFASTv2 models for XO-3 b. NEID radial velocity measurements are represented by inverted orange triangles, and previous measurements (Johns-Krull et al. 2008; Hébrard et al. 2008; Winn et al. 2009; Hirano et al. 2011a; Knutson et al. 2014; Bonomo et al. 2017; Garai et al. 2017; Worku et al. 2022) are shown in gray. *Lower panel:* Doppler Tomography signal for XO-3, obtained during transit. Our spectra captured by NEID produce the Doppler tomography seen in the left panel, while the best-fit model and associated residuals are shown in the middle and right panels, respectively.

Operations Center (SPOC; Jenkins et al. 2016) at NASA Ames Research Center. The data was downloaded using the `lightkurve` (Lightkurve Collaboration et al. 2018) Python package and includes 12 transits observed with 2-minute cadence across Sectors 19, 59, and 73, covering a four year time frame.

3. ATMOSPHERIC STELLAR PARAMETERS DERIVATION

To derive stellar atmospheric parameters such as T_{eff} , $[\text{Fe}/\text{H}]$, $\log g_*$, and $v \sin i_*$ for XO-3, we performed synthetic spectral fitting using `iSpec`² (Blanco-Cuaresma et al. 2014; Blanco-Cuaresma 2019) on the co-added out-of-transit NEID spectra ($\text{SNR}=258$). We adopted the SPECTRUM radiative transfer code (Gray & Corbally 1994), the MARCS atmosphere model (Gustafsson et al. 2008), and the sixth version of the GES atomic line list

(Heiter et al. 2021), all embedded in `iSpec`, to generate synthetic spectral models. Specific lines, including the wings of the $\text{H}\alpha$, $\text{H}\beta$, and Mg I triplet lines, as well as Fe I and Fe II lines, were selected to expedite the fitting process. We fixed the linear limb darkening coefficient and resolution at 0.6 and 110,000, respectively. The microturbulent velocity was treated as a free parameter, while the macroturbulent velocity was calculated using the empirical relation reported by Doyle et al. (2014). Using `iSpec`, we applied a nonlinear least-squares Levenberg–Marquardt algorithm (Moré 2006) to reduce the differences between the NEID and synthetic spectra. Upon achieving convergence, the uncertainty for each parameter was derived from the covariance matrix. The resulting parameters are listed in Table 2.

² <https://github.com/marblestation/iSpec>

4. GLOBAL MODELING

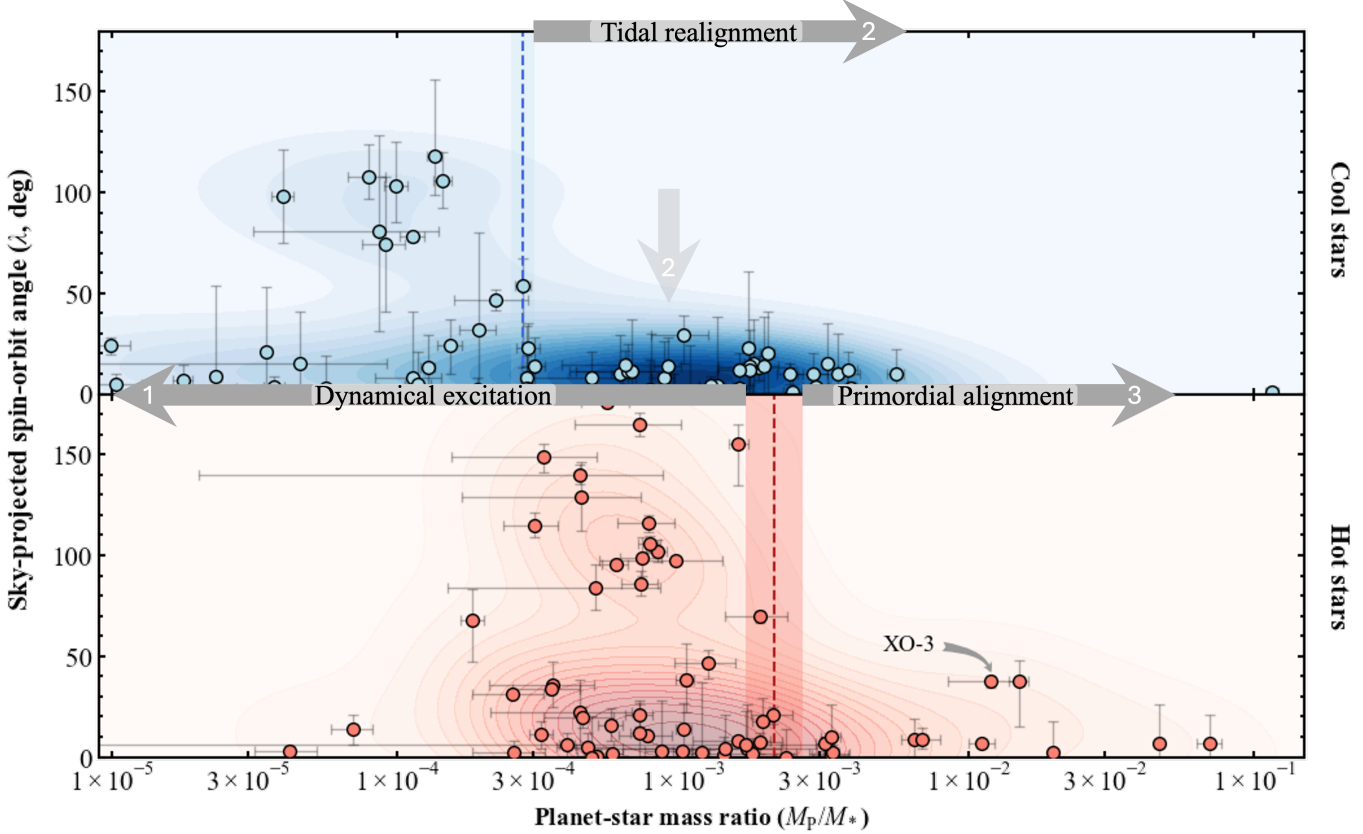


Figure 2. **Upper panel:** The sky-projected spin-orbit angle ($|\lambda|$) distribution for cool-star systems as a function of planet-to-star mass ratio. The contours represent the kernel density estimation of stellar obliquity measurements in the $M_p/M_*-|\lambda|$ space. The vertical blue dashed line marks the most likely boundary between the misalignment of low M_p/M_* systems and the alignment of high M_p/M_* systems. **Lower panel:** Similar to the upper panel, but for hot-star systems. The location of XO-3 is indicated by a curved gray arrow. The left-oriented arrow, marked as ‘1’, indicates that dynamical excitation can lead to misalignment in both cool-star and hot-star systems with $M_p/M_* < 2 \times 10^{-3}$. However, for cool stars with thick convective envelopes, misaligned systems with $3 \times 10^{-4} < M_p/M_* < 2 \times 10^{-3}$ are tidally damped, as shown by arrows marked as ‘2’. In systems with high mass ratios, represented by the ‘3’ arrow, primordial alignment dominates the stellar obliquity distribution, with no dynamical excitation causing misalignment. The data used to create this plot can be found via [this link](#).

To maintain consistency across both stellar and planetary parameters, we adopted EXOFASTv2³ (Eastman 2017; Eastman et al. 2019) to perform a global fit to the XO-3 spectral energy distribution (SED), transits, transit mid-times, and radial velocities (including the in-transit Rossiter-McLaughlin/Doppler Tomography measurements).

- MIST+SED modeling

To derive the system’s stellar parameters – particularly M_* , R_* , $\log g_*$, [Fe/H], and stellar age – we conducted SED fitting with the MESA Isochrones & Stellar Tracks (MIST; Choi et al. 2016; Dotter

2016) framework. The photometric magnitudes of XO-3 were compiled from multiple catalogues, including 2MASS (Cutri et al. 2003), WISE (Cutri et al. 2021), TESS (Ricker et al. 2015), and Gaia DR3 (Gaia Collaboration et al. 2023). Gaussian priors on T_{eff} and [Fe/H] were based on values from the NEID spectral analysis. We adopted an upper limit on the V-band extinction from Schlafly & Finkbeiner (2011) and a Gaussian prior on parallax from Gaia DR3 (Gaia Collaboration et al. 2023). Systematic uncertainty floors of 2.4% for bolometric flux and 2% for effective temperature, as suggested by Tayar et al. (2022), were applied.

- Photometry+out-of-transit RV modeling

The planetary parameters were derived from photometry and out-of-transit RV datasets. To expe-

³ Main branch: <https://github.com/jdeast/EXOFASTv2>; Version used in this work: <https://github.com/wangxianyu7/EXOFASTv2>.

Table 1. NEID Radial Velocities for the XO-3 System.

Time (BJD _{TDB})	RV (km s ⁻¹)	Error (km s ⁻¹)
2459514.68763608	-11.1265	0.0747
2459514.69556828	-11.1616	0.0647
2459514.70442987	-11.1867	0.0599
2459514.71321440	-11.2340	0.0591
2459514.72184409	-11.2649	0.0490
2459514.73043128	-11.2660	0.0471
2459514.73908392	-11.3376	0.0456
2459514.74766736	-11.3481	0.0447
2459514.75625436	-11.3862	0.0514
2459514.76509763	-11.3719	0.0544
2459514.77376901	-11.4033	0.0514
2459514.78217161	-11.4558	0.0465
2459514.79105276	-11.5296	0.0452
2459514.80988314	-11.6043	0.0484
2459514.81882804	-11.6420	0.0460
2459514.82741268	-11.7027	0.0426
2459514.83577554	-11.7092	0.0481
2459514.84486433	-11.7681	0.0454
2459514.85303856	-11.7761	0.0474
2459514.86193159	-11.7853	0.0493
2459514.87061424	-11.7555	0.0566
2459514.87959117	-11.7190	0.0540
2459514.88814168	-11.7648	0.0529
2459514.91309489	-11.8330	0.0410
2459514.92172524	-11.8595	0.0428
2459514.93557633	-11.8848	0.0431
2459514.94383404	-11.8944	0.0409

(This table is in machine-readable form in the online manuscript.)

dite the modeling process, the *TESS* photometry and ground-based transit mid-times from the literature, as reported by Ivshina & Winn (2022), were fitted simultaneously. *TESS* photometry provide a high-precision transit profile, and literature transit mid-times help to maintain an accurate ephemeris. The *TESS* light curve was detrended using the cosine method implemented in *wotan*⁴ (Hippke et al. 2019). Literature radial velocity data, which we leveraged to accurately constrain the planetary mass, eccentricity, and longitude of periastron, were obtained from the fol-

lowing spectrographs: the High Resolution Spectrograph (HRS) on the Hobby-Eberly Telescope and the Tull Coudé spectrograph on the Harlan J. Smith telescope (Tull et al. 1995; Tull 1998); the High Dispersion Spectrograph (HDS) on the Subaru telescope (Noguchi et al. 2002); the Spectrographe pour l’Observation des Phénomènes des Intérieurs stellaires et des Exoplanètes (SOPHIE) on the 1.93m reflector telescope at the Haute-Provence Observatory (Perruchot et al. 2008); the northern High Accuracy Radial velocity Planet Searcher (HARPS-N) on the Telescopio Nazionale Galileo (Cosentino et al. 2012, 2014); the Levy spectrograph on the Automated Planet Finder (APF) at Lick Observatory (Vogt et al. 2014); the HIgh Resolution Echelle Spectrometer (HIRES) on Keck I (Vogt et al. 2014); and the eShel spectrograph at Stara Lesna Observatory (Eversberg 2016). Uniform priors on planetary period, time of conjunction, planetary radius in stellar radii (R_P/R_*), semi-major axis in stellar radii (a/R_*), transformed eccentricity and longitude of periastron ($\sqrt{e} \cos \omega_*$ and $\sqrt{e} \sin \omega_*$), and impact parameter were applied. The priors on the quadratic limb-darkening coefficients (LDC) for *TESS* transits were interpolated using the Claret & Bloemen (2011) model based on the T_{eff} , [Fe/H], and $\log g_*$.

- RM modeling

To accurately model the RMs from Hébrard et al. (2008), Winn et al. (2010), Hirano et al. (2011a), and this work, we implemented one of the most realistic RM models presented by Hirano et al. (2011b), which accounts for stellar rotation, macroturbulence, thermal broadening, pressure broadening, and instrumental broadening. The V-band quadratic limb darkening coefficients were adopted, with priors interpolated using the Claret & Bloemen (2011) model based on T_{eff} , [Fe/H], and $\log g_*$. A Gaussian prior on $v \sin i_*$ was adopted based on the value derived from NEID spectral analysis (see Section 3). The prior on the macroturbulence velocity (v_ζ) was applied using the empirical equation described in Doyle et al. (2014). Uniform priors on the Gaussian dispersion (v_β) and Lorentzian dispersion (v_γ) were set to 2.5–4.5 km s⁻¹ and 0.5–1.5 km s⁻¹, respectively, consistent with the typical ranges presented by Hirano et al. (2011b).

- Doppler tomography modeling

Because of the fast rotation of XO-3 ($v \sin i_* \sim 18$ km s⁻¹), the line profile variation caused by the

⁴ <https://github.com/hippke/wotan>

transiting planet is significant. This enables a derivation of the projected spin-orbit angle using the Doppler tomography technique (Albrecht et al. 2007; Collier Cameron et al. 2010; Zhou et al. 2016; Johnson et al. 2017). To extract the Doppler tomography signal from NEID Level 2 data, we processed the CCF files by shifting their velocity coordinates to the stellar rest frame via subtraction of the systemic velocity. We then created a reference stellar line profile by averaging the out-of-transit CCFs. Subtracting this reference from the CCF of each observation isolated the DT signal of the planetary transit. Instead of adopting v_β , v_γ , and v_ζ , we introduced v_{line} to represent the average line width excluding the rotational broadening effect. A uniform prior of $2\text{--}10 \text{ km s}^{-1}$ was adopted for v_{line} . The prior on $v \sin i_*$ remains the same as in the RM modeling.

- Optimization and Uncertainty Sampling

We used EXOFASTv2 to simultaneously perform the aforementioned modeling and derive robust parameter uncertainties. First, EXOFASTv2 searched for initial guesses for floating parameters using the AMOEBA algorithm (Nelder & Mead 1965). Once AMOEBA found local minima, the Parallel Tempering Differential Evolution Markov Chain Monte Carlo (DE-MCMC; Ter Braak 2006) process was initiated with the best guesses. The MCMC procedure was considered converged when the Gelman-Rubin diagnostic (\hat{R} ; Gelman & Rubin 1992) fell below 1.01 and the count of independent draws surpassed 1000. The resulting parameters are listed in Table 2.

- Global modeling with different data combinations

To examine how sensitive the derived parameters are to different dataset combinations, we conducted four distinct global fits using varying datasets. All fits adopted *TESS* transits, literature transit mid-times, and RVs, with the differences arising from the usage of RMs and DT data. In the first case, we performed a fit using all literature RMs combined with the DT data from this work (denoted as “Literature RMs + NEID DT”). In the second case, we included all RMs, including those newly collected in this work (“Literature RMs + NEID RM”). In the third case, we used only our NEID DT data without any additional RMs (“NEID DT”). In the last case, we used only the NEID RM data (“NEID RM”). To maintain consistency with the results from RM modeling in

the literature, we adopt the results from the “Literature RMs + NEID RM” fit, which yields an RM SNR of 338 (Kipping 2023; Kipping & Wang 2024) and $\lambda = 41.8^{+2.1}_{-2.0} \text{ }^\circ$. The results of each of the four fits are listed in Table 2.

We found that the resulting system parameters are in good agreement with values derived in previous studies (differences within $\lesssim 2\sigma$), except for the stellar effective temperature and radius. The stellar T_{eff} derived from our analysis is consistent (within 1σ) with the values reported by Tsantaki et al. (2014), *Gaia* DR2 (Gaia Collaboration et al. 2018), *Gaia* DR3 (Gaia Collaboration et al. 2023), and the TIC catalog (Stassun & Torres 2018), but differs by 2.4σ from the value reported by Johns-Krull et al. (2008). This discrepancy may be attributable to differences in data quality and spectral analysis software. For stellar radius, the 2.8σ inconsistency may originate from differences in parallax between *Gaia* DR2 and DR3. Previous studies (e.g. Worku et al. (2022)) adopted the *Gaia* DR2 (Gaia Collaboration et al. 2016) parallax ($4.66 \pm 0.06 \text{ mas}$), which differs significantly from the *Gaia* DR3 parallax ($4.86 \pm 0.03 \text{ mas}$) used in this work. Notably, our λ and $v \sin i_*$ agree with values from previous accurate measurements (Winn et al. 2009: $\lambda = 37.3 \pm 3.7^\circ$, $v \sin i_* = 17.0 \pm 1.2 \text{ km s}^{-1}$; Hirano et al. 2011a: $\lambda = 37.3 \pm 3.0^\circ$, $v \sin i_* = 18.54 \pm 0.17 \text{ km s}^{-1}$) within 1.3σ .

In some cases, the true stellar obliquity ψ can be determined if the stellar rotational velocity v is inferred from photometric variability caused by long-lived starspots on the surface of the host star (e.g. Mancini et al. (2015), Bourrier et al. (2018), Stefansson et al. (2022)). Therefore, we applied the autocorrelation function embedded in SpinSpotter (Holcomb et al. 2022) to the *TESS* light curve. We did not detect any significant periodic signal; therefore, the true stellar obliquity of XO-3 cannot yet be determined.

5. POPULATION ANALYSIS

Previous studies (e.g. Hébrard et al. (2011), Triaud (2018), Zhou et al. (2019a), Albrecht et al. (2022), Hixenbaugh et al. (2023), Gan et al. (2024)) reported tentative evidence for a trend toward alignment in massive planet ($M_P \gtrsim 3 M_J$) or high M_P/M_* ($M_P/M_* > 2 \times 10^{-3}$) systems. However, historically, a limited sample size has made the statistical validation of this trend uncertain. Recently, the sample of high M_P/M_* systems has been rapidly expanding, benefiting from *TESS*,

which has uncovered numerous such systems and facilitated a series of follow-up stellar obliquity observations (e.g., LP 261-75A b, [Brady et al. \(2024\)](#); TOI-2119 b, [Doyle et al. \(2024\)](#); TOI-2145, [Dong et al. \(2024\)](#); TOI-2533, [Schmidt et al. \(2023\)](#); Ferreira dos Santos et al. (2024); TOI-3362, [Dong et al. \(2021\)](#); Espinoza-Retamal et al. (2023); TOI-4603, [Khandelwal et al. \(2023\)](#); TIC 241249530, [Gupta et al. \(2024\)](#); GPX-1, [Benni et al. \(2021\)](#); Giacalone et al. (2024)). We revisit the M_p/M_* trend in light of these new measurements.

- Sample construction

In this work, using literature stellar obliquities from TEPCat⁵ ([Southworth 2011](#)) and recent studies including [Knudstrup et al. \(2024\)](#), [Dong et al. \(2024\)](#), [Brady et al. \(2024\)](#), and [Doyle et al. \(2024\)](#), we conducted a population-level analysis to re-investigate the tentative alignment trend in single-star, high M_p/M_* systems. For each system, we used the preferred values for λ and T_{eff} from the TEPCat catalog, while M_* and M_p were sourced from the Planetary Systems Composite Data table in the NASA Exoplanet Archive⁶. To maintain the purity of the sample, following the first three criteria of the sample construction procedure outlined in Appendix B of [Wang et al. \(2024\)](#), we included only stellar obliquity measurements obtained using the Rossiter-McLaughlin or Doppler tomography techniques, while excluding low-quality and contested measurements, as well as systems containing binary or multiple stars. We also excluded systems with planetary masses that have only upper or lower limits.

This procedure resulted in 135 systems, including 7 brown dwarf systems (CoRoT-3, [Triaud et al. \(2009\)](#); GPX-1, [Giacalone et al. \(2024\)](#); KELT-1, [Siverd et al. \(2012\)](#); TOI-2119, [Doyle et al. \(2024\)](#); TOI-2533, [Ferreira dos Santos et al. \(2024\)](#); WASP-30, [Triaud et al. \(2013\)](#), and XO-3). Among them, 71 systems include cool host stars ($T_{\text{eff}} < 6100$ K), while 64 systems include hot host stars ($T_{\text{eff}} \geq 6100$ K). The resulting sky-projected stellar obliquity distribution is shown in Figure 2. There are clear differences in the obliquity distributions between systems with low and high M_p/M_* ratios in both the hot and cool star samples.

⁵ Accessed on November 17, 2024, at <https://www.astro.keele.ac.uk/jkt/tepcat/obliquity.html>.

⁶ <https://exoplanetarchive.ipac.caltech.edu/cgi-bin/TblView/nph-TblView?app=ExoTbls&config=PSCCompPars>

- Empirical boundary

To determine the empirical threshold that distinguishes the λ distributions of systems with low and high M_p/M_* ratios, we applied a Anderson-Darling test (AD; [Scholz & Stephens 1987](#)) implemented in `scipy` ([Virtanen et al. 2020](#)). The null hypothesis assumes that the stellar obliquity distributions on both sides of the boundary are identical. For each iteration, random λ values were drawn for the systems, incorporating the reported Gaussian uncertainties for each measurement. The boundary value was varied logarithmically from 10^{-4} to 10^{-1} with a step size of 0.001, and the boundary with most significant AD statistic was recorded. This process was repeated 1,000 times to generate the AD statistic distribution as a function of M_p/M_* , which was fitted with a Gaussian profile to determine the median value and 1σ uncertainty for boundaries. This procedure was applied separately to the cool-star and hot-star systems, resulting in M_p/M_* boundaries of 0.00027 ± 0.00002 and $0.0021^{+0.0006}_{-0.0008}$, respectively.

- Statistical significance

For the cool star sample (as shown in the top panel of Figure 2), there are 31 systems with $M_p/M_* < 3 \times 10^{-4}$ spanning a range of spin-orbit orientations. In contrast, 40 systems with $M_p/M_* \geq 3 \times 10^{-4}$ are generally well aligned. Considering the similar sample sizes of the low M_p/M_* and high M_p/M_* groups, we applied the AD test and a Monte Carlo approach to compare the distributions of the two groups while accounting for stellar obliquity uncertainties. The null hypothesis is that the two samples originate from the same distribution. In each iteration, Gaussian noise was introduced to simulate measurement errors, and the p-value of the AD test was calculated. This process was repeated 100,000 times to build a robust distribution of AD p-values. The results show that 97.8% of the resultant p-values are less than 0.05, strongly rejecting the null hypothesis and indicating that, for the stellar obliquity distribution of cool stars, low M_p/M_* and high M_p/M_* systems are distinct.

For the hot star sample (as shown in the bottom panel of Figure 2), there are 50 systems with $M_p/M_* < 2 \times 10^{-3}$, spanning a range of spin-orbit orientations, while 14 systems with $M_p/M_* \geq 2 \times 10^{-3}$ tend to have low stellar obliquity. Similar to the cool star sample, a comparable AD test analysis was conducted for the hot star sample, showing

that 85.9% of the resultant p-values are less than 0.05, suggesting an intrinsic difference between low M_P/M_* and high M_P/M_* systems with hot stars. Due the highly uneven sample size, we also employed a bootstrapping method to assess the significance of the observed alignment trend in high M_P/M_* systems. Following Wang et al. (2022), Rice et al. (2022b), and Wang et al. (2024), we define “misaligned” systems as those with $|\lambda| > 10^\circ$ and λ deviating from 0° at a 3σ significance level. Specifically, we iteratively draw random samples of 14 $|\lambda|$ values from the hot-star low M_P/M_* sample without replacement to determine how many are misaligned. This process is repeated 100,000 times to establish a stable distribution for the number of misaligned systems. The results demonstrate that the difference in the spin-orbit distribution between hot-star low M_P/M_* and high M_P/M_* systems is significant at the 3.7σ level.

The boundaries derived from our work are similar to those reported by Albrecht et al. (2022). However, Albrecht et al. (2022) found that the suggestive alignment in high M_P/M_* systems does not hold for very hot stars ($T_{\text{eff}} > 7000$ K). We, therefore, examined the misaligned systems with very hot stars ($T_{\text{eff}} > 7000$ K) shown in the lower panel of Figure 9 in Albrecht et al. (2022), and found that all misaligned systems with $M_P/M_* \geq 2 \times 10^{-3}$ are either in binary systems (Kepler-13, Borucki et al. (2011); KELT-19, Siverd et al. (2018)) or have only upper limits on their planetary masses (HAT-P-70, Zhou et al. (2019b); WASP-167, Temple et al. (2017)).

- XO-3: Exception

Among single-star systems with high M_P/M_* —which are typically well-aligned—XO-3 b stands out as a notable exception. It possesses an unusually large planet-star mass ratio ($M_P/M_* = 9 \times 10^{-3}$) and exhibits a high stellar obliquity ($\lambda = 41.8^{+2.1}_{-2.0}{}^\circ$), presenting a significant challenge in understanding its dynamical history (Johns-Krull et al. 2008; Hébrard et al. 2008; Winn et al. 2009; Hirano et al. 2011a; Worku et al. 2022). We, therefore, consider the possibility that the system har-

bors an undetected stellar companion that may have misaligned the system (e.g. Wu & Murray 2003; Fabrycky & Tremaine 2007; Hjorth et al. 2021; Espinoza-Retamal et al. 2023; Su & Lai 2024).

To search for a potential stellar companion, we first applied the RV planet search pipeline, `rvsearch`⁷ (Rosenthal et al. 2021) based on RadVel (Fulton et al. 2018), to the residual RV data obtained after removing the signal induced by XO-3 b. Although Hirano et al. (2011a) identified a tentative linear trend in radial velocity data from Subaru/HDS and OHP/SOPHIE, our analysis found no significant signals with a false alarm probability below 0.1. This suggests either the absence of a nearby companion or an insufficient number or precision of RVs to detect one. Unfortunately, due to the lack of high-precision astrometry measurements in the Hipparcos catalog (ESA 1997), Hipparcos+*Gaia* astrometry detection cannot be achieved.

Previous imaging observations of XO-3 did not find a physically associated stellar companion (Lucky Imaging by AstraLux Norte (Bergfors et al. 2013; Wöllert & Brandner 2015); direct imaging by Keck/NIRC2 (Ngo et al. 2015)). However, *Gaia* DR3 (Gaia Collaboration et al. 2023) reports that XO-3 has a Renormalized Unit Weight Error RUWE; (RUWE; Lindegren et al. 2018, 2021) of 1.25, suggesting a poor astrometric solution, whereas RUWE is typically close to unity for single stars with reliable astrometric data. A high RUWE (> 1.2) indicates a strong likelihood of a nearby unresolved stellar companion (Belokurov et al. 2020; Krolikowski et al. 2021), although other factors, such as circumstellar material (Fittin et al. 2022), can also contribute to an elevated RUWE. The potential presence of a stellar companion can be tested with the upcoming *Gaia* DR4 epoch data. If the binary nature of XO-3 is confirmed, it would no longer represent the only known misaligned single-star system with $M_P/M_* \geq 2 \times 10^{-3}$. The statistical significance of alignment in high M_P/M_* single-star systems would, in this case, increase from 3.7σ to 4.1σ .

⁷ <https://github.com/California-Planet-Search/rvsearch>

Table 2. Median values and 68% confidence interval for combined parameters.

Parameter	Description	Values			
Stellar parameters from iSpec fit:					
T_{eff}	Effective Temperature (K)	6784 ± 141			
[Fe/H]	Metallicity (dex)	-0.23 ± 0.09			
$\log g$	Surface Gravity (cgs)	4.05 ± 0.32			
$v \sin i_*$	Projected rotational velocity (m/s)	19.28 ± 1.61			
EXOFASTv2 fit:					
Stellar Parameters:					
M_*	Mass (M_{\odot})	$1.41^{+0.067}_{-0.069}$	$1.409^{+0.066}_{-0.07}$	$1.433^{+0.066}_{-0.07}$	$1.424^{+0.066}_{-0.07}$
R_*	Radius (R_{\odot})	$1.52^{+0.029}_{-0.03}$	$1.508^{+0.029}_{-0.03}$	$1.524^{+0.029}_{-0.03}$	$1.515^{+0.029}_{-0.03}$
L_*	Luminosity (L_{\odot})	$1.582^{+0.034}_{-0.032}$	$1.583^{+0.034}_{-0.033}$	$1.57^{+0.034}_{-0.032}$	$1.575^{+0.034}_{-0.033}$
F_{Bol}	Bolometric Flux (cgs)	$3.17^{+0.25}_{-0.23}$	$3.09^{+0.24}_{-0.23}$	$3.47^{+0.32}_{-0.3}$	$3.3^{+0.28}_{-0.27}$
ρ_*	Density (cgs)	$0.565^{+0.024}_{-0.022}$	$0.578^{+0.024}_{-0.023}$	$0.569^{+0.024}_{-0.023}$	$0.577^{+0.024}_{-0.023}$
$\log g$	Surface Gravity (cgs)	$4.223^{+0.014}_{-0.015}$	$4.23^{+0.014}_{-0.014}$	$4.227^{+0.015}_{-0.015}$	$4.23^{+0.014}_{-0.015}$
T_{eff}	Effective Temperature (K)	6790^{+100}_{-110}	6770^{+100}_{-100}	6940^{+130}_{-130}	6870^{+120}_{-120}
[Fe/H]	Metallicity (dex)	$-0.131^{+0.089}_{-0.11}$	$-0.122^{+0.088}_{-0.11}$	$-0.166^{+0.097}_{-0.12}$	$-0.146^{+0.092}_{-0.12}$
Age	Age (Gyr)	$1.25^{+0.54}_{-0.4}$	$1.2^{+0.54}_{-0.39}$	$1.09^{+0.47}_{-0.35}$	$1.11^{+0.49}_{-0.37}$
EEP	Equal Evolutionary Phase	$339.7^{+8.4}_{-10.0}$	$338.2^{+8.9}_{-10.0}$	$337.2^{+8.6}_{-11.0}$	$337.0^{+8.8}_{-11.0}$
A_V	V-band Extinction (mag)	$0.16^{+0.15}_{-0.11}$	$0.14^{+0.15}_{-0.1}$	$0.16^{+0.15}_{-0.11}$	$0.18^{+0.15}_{-0.12}$
ϖ	Parallax (mas)	$4.74^{+0.064}_{-0.064}$	$4.745^{+0.063}_{-0.063}$	$4.731^{+0.064}_{-0.064}$	$4.738^{+0.064}_{-0.064}$
d	Distance (pc)	$211.0^{+2.9}_{-2.8}$	$210.8^{+2.8}_{-2.8}$	$211.4^{+2.9}_{-2.8}$	$211.1^{+2.9}_{-2.8}$
Rossiter-McLaughlin and Doppler Tomography Parameters:					
λ	Projected spin-orbit angle (deg) ...	$39.5^{+1.4}_{-1.4}$	$41.8^{+2.1}_{-2.0}$	$39.5^{+1.6}_{-1.6}$	$37.1^{+5.1}_{-4.8}$
$v \sin i_*$	Projected rotational velocity (m/s)	18050^{+230}_{-230}	18630^{+240}_{-240}	17290^{+380}_{-380}	18550^{+490}_{-500}
v_{line}	Unbroadened line width (m/s)....	8590^{+540}_{-510}	...	8250^{+550}_{-520}	...
v_{β}	Gaussian dispersion (m/s)	3790^{+520}_{-750}	3640^{+600}_{-710}	3500^{+680}_{-680}	3490^{+690}_{-680}
v_{γ}	Lorentzian dispersion (m/s)	1060^{+300}_{-360}	1010^{+340}_{-340}	1000^{+340}_{-340}	1000^{+340}_{-340}
v_{ζ}	Macroturbulence dispersion (m/s) .	6170^{+240}_{-490}	6150^{+260}_{-510}	4300^{+1500}_{-1500}	5640^{+630}_{-1100}
Planetary Parameters:					
P	Period (days)	$3.19152313^{+1.5e-07}_{-1.5e-07}$	$3.19152308^{+1.5e-07}_{-1.4e-07}$	$3.19152307^{+1.5e-07}_{-1.5e-07}$	$3.19152306^{+1.5e-07}_{-1.5e-07}$
R_P	Radius (R_J)	$1.317^{+0.027}_{-0.027}$	$1.307^{+0.027}_{-0.028}$	$1.32^{+0.027}_{-0.028}$	$1.312^{+0.027}_{-0.028}$
M_P	Mass (M_J)	$13.03^{+0.41}_{-0.43}$	$13.03^{+0.41}_{-0.43}$	$13.18^{+0.4}_{-0.44}$	$13.13^{+0.4}_{-0.43}$
T_C	Time of conjunction - 2457417....	$0.98762^{+0.00011}_{-0.00011}$	$0.9876^{+0.00011}_{-0.00011}$	$0.98762^{+0.00011}_{-0.00011}$	$0.98761^{+0.00011}_{-0.00011}$
a	Semi-major axis (AU)	$0.04771^{+0.00074}_{-0.00079}$	$0.0477^{+0.00073}_{-0.0008}$	$0.04796^{+0.00072}_{-0.0008}$	$0.04787^{+0.00072}_{-0.00079}$
i	Inclination (Degrees)	$83.57^{+0.18}_{-0.17}$	$83.67^{+0.17}_{-0.17}$	$83.6^{+0.18}_{-0.18}$	$83.66^{+0.18}_{-0.18}$
e	Eccentricity	$0.2795^{+0.0026}_{-0.0024}$	$0.279^{+0.0024}_{-0.0023}$	$0.2785^{+0.0026}_{-0.0024}$	$0.2784^{+0.0025}_{-0.0023}$
ω_*	Arg of periastron (Degrees)	$-11.08^{+0.86}_{-0.95}$	$-10.77^{+0.76}_{-0.82}$	$-10.54^{+0.88}_{-0.95}$	$-10.51^{+0.83}_{-0.89}$
R_P/R_*	Radius of planet in stellar radii ...	$0.08906^{+0.00026}_{-0.00027}$	$0.08906^{+0.00028}_{-0.00028}$	$0.08897^{+0.00027}_{-0.00027}$	$0.08901^{+0.00028}_{-0.00028}$
a/R_*	Semi-major axis in stellar radii	$6.747^{+0.094}_{-0.09}$	$6.797^{+0.093}_{-0.091}$	$6.762^{+0.095}_{-0.092}$	$6.791^{+0.095}_{-0.093}$
T_{14}	Total transit duration (days)	$0.12366^{+0.00047}_{-0.00047}$	$0.12351^{+0.00047}_{-0.00047}$	$0.10321^{+0.00049}_{-0.00049}$	$0.12351^{+0.00048}_{-0.00047}$
b	Transit impact parameter	$0.7366^{+0.0093}_{-0.01}$	$0.7295^{+0.0098}_{-0.01}$	$0.7329^{+0.0097}_{-0.010}$	$0.729^{+0.01}_{-0.01}$
$\sqrt{e} \cos \omega_*$..	Eccentricity parameter 1	$0.5188^{+0.0015}_{-0.0014}$	$0.5188^{+0.0015}_{-0.0014}$	$0.5188^{+0.0015}_{-0.0015}$	$0.5187^{+0.0015}_{-0.0014}$
$\sqrt{e} \sin \omega_*$..	Eccentricity parameter 2	$-0.1016^{+0.0082}_{-0.009}$	$-0.0987^{+0.0072}_{-0.0078}$	$-0.0966^{+0.0083}_{-0.0090}$	$-0.0962^{+0.0078}_{-0.0084}$
u_{l0}	Linear LDC for TESS.....	$0.139^{+0.037}_{-0.037}$	$0.159^{+0.036}_{-0.036}$	$0.286^{+0.042}_{-0.042}$	$0.153^{+0.036}_{-0.037}$
u_{20}	Quadratic LDC for TESS.....	$0.275^{+0.042}_{-0.041}$	$0.274^{+0.042}_{-0.042}$	$0.286^{+0.042}_{-0.042}$	$0.282^{+0.042}_{-0.042}$
u_{l1}	Linear LDC for RMs	$0.243^{+0.016}_{-0.015}$	$0.253^{+0.015}_{-0.014}$...	$0.217^{+0.017}_{-0.017}$
u_{21}	Quadratic LDC for RMs	$0.306^{+0.015}_{-0.015}$	$0.304^{+0.012}_{-0.013}$...	$0.301^{+0.017}_{-0.017}$

6. SUMMARY AND IMPLICATIONS

Perhaps the most significant trend in stellar obliquity studies is that hot Jupiters — Jupiter-mass planets, defined in our study as planets with a planet-to-star mass ratio $3 \times 10^{-4} \lesssim M_p/M_* \lesssim 2 \times 10^{-3}$, on short orbital periods ($a/R_* < 11$; Rice et al. 2021, 2022b; Wang et al. 2022, 2024) — tend to be aligned with cool host stars, whereas they are often misaligned with hot stars (Winn et al. 2010). This temperature-obliquity ($T_{\text{eff}} - \lambda$) relationship is widely attributed to tidal damping mechanisms (Albrecht et al. 2012; Li & Winn 2016; Wang et al. 2021; Rice et al. 2022a; Zanazzi et al. 2024), which may be sufficiently strong to realign the obliquity of cool stars, but which are less effective around hotter stars.

The tidal realignment scenario also explains why planets with masses lower than Jupiter’s — predominantly sub-Saturns (as shown in the upper panel of Figure 2, with $M_p/M_* < 3 \times 10^{-4}$) — consistently exhibit misalignments even around cool stars. Their low planetary masses correspond to long tidal realignment timescales, such that the systems would remain misaligned even if the host stars have thick convective envelopes and/or small radiative cores (Albrecht et al. 2012; Zanazzi et al. 2024).

However, the tidal realignment mechanism alone cannot fully explain the trend reported in this study:

We find that single-star systems with high planet-to-star mass ratios ($M_p/M_* \geq 2 \times 10^{-3}$) tend to be aligned even around hot stars. This is a 3.7σ deviation from the stellar obliquity distribution of planets with lower mass ratios ($M_p/M_* < 2 \times 10^{-3}$), as shown in the lower panel of Figure 2.

Since tidal realignment is inefficient for hot stars (Albrecht et al. 2012; Zanazzi et al. 2024) — making it unlikely that these systems are realigned through tidal interactions — alignment for $M_p/M_* \geq 2 \times 10^{-3}$ systems is likely primordial.

The empirical boundary between primordially aligned high-mass-ratio systems ($M_p/M_* \geq 2 \times 10^{-3}$) and often-misaligned low-mass-ratio systems ($M_p/M_* < 2 \times 10^{-3}$) suggests that stellar obliquities are more prone to excitation in systems with low planet-to-star mass ratios. Stellar obliquity measurements of compact multi-planet systems and warm Jupiters around single stars — which are consistently aligned (Albrecht et al. 2013; Wang et al. 2018; Zhou et al. 2018; Radzom et al. 2024; Rice et al. 2022b, 2023b; Wang et al. 2024) — disfavor the possibility of primordial protoplanetary disk misalignments. Therefore, observed spin-orbit misalignments in systems

with low planet-to-star mass ratios are likely caused by dynamical instabilities involving other planets that were originally in relatively compact configurations (Rasio & Ford 1996; Goldreich et al. 2004; Chatterjee et al. 2008; Nagasawa et al. 2008; Nagasawa & Ida 2011; Beaugé & Nesvorný 2012; Xu & Wang 2024). The largest planet mass achievable in a compact system through core accretion is limited by the gap-opening mass (Ginzburg & Chiang 2019), which may align with the empirical boundary $M_p/M_* = 2 \times 10^{-3}$ identified between aligned high M_p/M_* systems and misaligned low M_p/M_* systems. Above this boundary, system would more easily become unstable, which would halt further gas accretion and prevents the formation of higher mass-ratio systems through this mechanism.

Systems with high planet-to-star mass ratios — such as those with brown dwarf companions, or M-dwarfs hosting Jupiter-like planets — may not form in compact configurations and would instead remain dynamically cool. Without nearby companions, dynamically isolated planets may continue to accrete gas through their circumplanetary disks even as accretion slows due to gap opening (Benisty et al. 2021; Aoyama & Ikoma 2019; Toci et al. 2020), which allows these planets to evolve into super-Jupiters while they maintain their primordial alignment. Alternatively, for the highest planet-to-star mass ratio objects under consideration ($M_p/M_* \geq 2 \times 10^{-3}$), disk fragmentation becomes an increasingly plausible formation mechanism (Xu et al. 2024). However, the extent of the objects’ migration from the outer regions of the disk (Zhu et al. 2012; Galvagni & Mayer 2014), where fragmentation occurs, and whether they can avoid significant perturbations and maintain low obliquities, remain uncertain.

Overall, we suggest that planets with $M_p/M_* < 2 \times 10^{-3}$ may form in compact multi-planet systems and dynamical instabilities sculpt their properties, resulting in a spectrum of system architectures (Wu et al. 2023). These range from hyper-stable “peas-in-a-pod” systems (Weiss et al. 2018; Millholland et al. 2017; Wang 2017; Goyal & Wang 2022) — particularly those still locked in resonance chains (Goyal et al. 2023; Schmidt et al. 2024; Dai et al. 2024), which tend to be aligned (Wang et al. 2018; Rice et al. 2023b; Dai et al. 2023) — to metastable configurations, such as ultra-short-period planets (Dai et al. 2018) and Mercury in our Solar System (Lithwick & Wu 2014), which have been found to have large inclinations. In some systems with $M_p/M_* < 2 \times 10^{-3}$, violent planet-planet interactions significantly increase a system’s dynamical temperature, elevating orbital eccentricities and inclinations. A subset of such systems may then be dynamically cooled through tidal circular-

ization (becoming hot Jupiters) and realignment processes, culminating in the currently observed distribution.

In contrast, systems with $M_P/M_* \geq 2 \times 10^{-3}$ may have formed in more isolated environments. Without dynamical perturbations from compact companions, these planets could maintain their primordial alignment and continue growing on their own.

We thank Wenrui Xu, Cristobal Petrovich, and Bonan Pu for their insightful discussions.

M.R. acknowledges support from Heising-Simons Foundation grant #2023-4478 and the National Geographic Society. S.W. acknowledges support from Heising-Simons Foundation grant #2023-4050. We acknowledge support from the NASA Exoplanets Research Program NNH23ZDA001N-XRP (grant #80NSSC24K0153).

Funding for the *TESS* mission is provided by NASA’s Science Mission directorate. This paper includes data collected by the *TESS* mission, which are publicly available from the Mikulski Archive for Space Telescopes (MAST).

This work has made use of data from the European Space Agency (ESA) mission *Gaia* (<https://www.cosmos.esa.int/gaia>), processed by the *Gaia* Data Processing and Analysis Consortium (DPAC, <https://www.cosmos.esa.int/web/gaia/dpac/consortium>). Funding for the DPAC has been provided by national institutions, in particular the institutions participating in the *Gaia* Multilateral Agreement.

This research was supported in part by Lilly Endowment, Inc., through its support for the Indiana University Pervasive Technology Institute.

Facilities: WIYN/NEID, TESS (doi:10.17909/njj7-v638) , IAPC (doi:10.26133/NEA2)

Software: EXOFASTv2 (Eastman 2017; Eastman et al. 2019), iSpec (Blanco-Cuaresma et al. 2014; Blanco-Cuaresma 2019), lightkurve (Lightkurve Collaboration et al. 2018), matplotlib (Hunter 2007), numpy (Oliphant 2006; Walt et al. 2011; Harris et al. 2020), pandas (McKinney 2010), scipy (Virtanen et al. 2020), SpinSpotter (Holcomb et al. 2022).

REFERENCES

- Albrecht, S., Reffert, S., Quirrenbach, A., Mitchell, D. S., & Snellen, I. 2007, in Astronomical Society of the Pacific Conference Series, Vol. 370, Solar and Stellar Physics Through Eclipses, ed. O. Demircan, S. O. Selam, & B. Albayrak, 218
- Albrecht, S., Winn, J. N., Marcy, G. W., et al. 2013, ApJ, 771, 11, doi: [10.1088/0004-637X/771/1/11](https://doi.org/10.1088/0004-637X/771/1/11)
- Albrecht, S., Winn, J. N., Johnson, J. A., et al. 2012, ApJ, 757, 18, doi: [10.1088/0004-637X/757/1/18](https://doi.org/10.1088/0004-637X/757/1/18)
- Albrecht, S. H., Dawson, R. I., & Winn, J. N. 2022, PASP, 134, 082001, doi: [10.1088/1538-3873/ac6c09](https://doi.org/10.1088/1538-3873/ac6c09)
- Anderson, K. R., Winn, J. N., & Penev, K. 2021, ApJ, 914, 56, doi: [10.3847/1538-4357/abf8af](https://doi.org/10.3847/1538-4357/abf8af)
- Aoyama, Y., & Ikoma, M. 2019, ApJL, 885, L29, doi: [10.3847/2041-8213/ab5062](https://doi.org/10.3847/2041-8213/ab5062)
- Beaugé, C., & Nesvorný, D. 2012, ApJ, 751, 119, doi: [10.1088/0004-637X/751/2/119](https://doi.org/10.1088/0004-637X/751/2/119)
- Belokurov, V., Penoyre, Z., Oh, S., et al. 2020, MNRAS, 496, 1922, doi: [10.1093/mnras/staa1522](https://doi.org/10.1093/mnras/staa1522)
- Benisty, M., Bae, J., Facchini, S., et al. 2021, ApJL, 916, L2, doi: [10.3847/2041-8213/ac0f83](https://doi.org/10.3847/2041-8213/ac0f83)
- Benni, P., Burdanov, A. Y., Krushinsky, V. V., et al. 2021, MNRAS, 505, 4956, doi: [10.1093/mnras/stab1567](https://doi.org/10.1093/mnras/stab1567)
- Bergfors, C., Brandner, W., Daemgen, S., et al. 2013, MNRAS, 428, 182, doi: [10.1093/mnras/sts019](https://doi.org/10.1093/mnras/sts019)
- Blanco-Cuaresma, S. 2019, MNRAS, 486, 2075, doi: [10.1093/mnras/stz549](https://doi.org/10.1093/mnras/stz549)
- Blanco-Cuaresma, S., Soubiran, C., Heiter, U., & Jofré, P. 2014, A&A, 569, A111, doi: [10.1051/0004-6361/201423945](https://doi.org/10.1051/0004-6361/201423945)
- Bonomo, A. S., Desidera, S., Benatti, S., et al. 2017, A&A, 602, A107, doi: [10.1051/0004-6361/201629882](https://doi.org/10.1051/0004-6361/201629882)
- Borucki, W. J., Koch, D. G., Basri, G., et al. 2011, ApJ, 736, 19, doi: [10.1088/0004-637X/736/1/19](https://doi.org/10.1088/0004-637X/736/1/19)
- Bourrier, V., Lovis, C., Beust, H., et al. 2018, Nature, 553, 477, doi: [10.1038/nature24677](https://doi.org/10.1038/nature24677)
- Brady, M., Bean, J., Stefánsson, G., et al. 2024, arXiv e-prints, arXiv:2411.10402, doi: [10.48550/arXiv.2411.10402](https://doi.org/10.48550/arXiv.2411.10402)
- Chatterjee, S., Ford, E. B., Matsumura, S., & Rasio, F. A. 2008, ApJ, 686, 580, doi: [10.1086/590227](https://doi.org/10.1086/590227)
- Choi, J., Dotter, A., Conroy, C., et al. 2016, ApJ, 823, 102, doi: [10.3847/0004-637X/823/2/102](https://doi.org/10.3847/0004-637X/823/2/102)
- Claret, A., & Bloemen, S. 2011, A&A, 529, A75, doi: [10.1051/0004-6361/201116451](https://doi.org/10.1051/0004-6361/201116451)
- Collier Cameron, A., Bruce, V. A., Miller, G. R. M., Triaud, A. H. M. J., & Queloz, D. 2010, MNRAS, 403, 151, doi: [10.1111/j.1365-2966.2009.16131.x](https://doi.org/10.1111/j.1365-2966.2009.16131.x)
- Cosentino, R., Lovis, C., Pepe, F., et al. 2012, in Society of Photo-Optical Instrumentation Engineers (SPIE) Conference Series, Vol. 8446, Ground-based and Airborne Instrumentation for Astronomy IV, ed. I. S. McLean, S. K. Ramsay, & H. Takami, 84461V, doi: [10.1117/12.925738](https://doi.org/10.1117/12.925738)
- Cosentino, R., Lovis, C., Pepe, F., et al. 2014, in Society of Photo-Optical Instrumentation Engineers (SPIE) Conference Series, Vol. 9147, Ground-based and Airborne Instrumentation for Astronomy V, ed. S. K. Ramsay, I. S. McLean, & H. Takami, 91478C, doi: [10.1117/12.2055813](https://doi.org/10.1117/12.2055813)
- Cutri, R. M., Skrutskie, M. F., van Dyk, S., et al. 2003, VizieR Online Data Catalog, II/246
- Cutri, R. M., Wright, E. L., Conrow, T., et al. 2021, VizieR Online Data Catalog, II/328
- Dai, F., Masuda, K., & Winn, J. N. 2018, ApJL, 864, L38, doi: [10.3847/2041-8213/aadd4f](https://doi.org/10.3847/2041-8213/aadd4f)
- Dai, F., Masuda, K., Beard, C., et al. 2023, AJ, 165, 33, doi: [10.3847/1538-3881/aca327](https://doi.org/10.3847/1538-3881/aca327)
- Dai, F., Goldberg, M., Batygin, K., et al. 2024, AJ, 168, 239, doi: [10.3847/1538-3881/ad83a6](https://doi.org/10.3847/1538-3881/ad83a6)
- de Laplace, P. S. 1796, Exposition du système du monde, doi: [10.3931/e-rara-497](https://doi.org/10.3931/e-rara-497)
- Dong, J., Huang, C. X., Zhou, G., et al. 2021, ApJL, 920, L16, doi: [10.3847/2041-8213/ac2600](https://doi.org/10.3847/2041-8213/ac2600)
- Dong, J., Wang, S., Rice, M., et al. 2023, arXiv e-prints, arXiv:2305.16495, doi: [10.48550/arXiv.2305.16495](https://doi.org/10.48550/arXiv.2305.16495)
- Dong, J., Chontos, A., Zhou, G., et al. 2024, arXiv e-prints, arXiv:2411.01356, doi: [10.48550/arXiv.2411.01356](https://doi.org/10.48550/arXiv.2411.01356)
- Dotter, A. 2016, ApJS, 222, 8, doi: [10.3847/0067-0049/222/1/8](https://doi.org/10.3847/0067-0049/222/1/8)
- Doyle, A. P., Davies, G. R., Smalley, B., Chaplin, W. J., & Elsworth, Y. 2014, MNRAS, 444, 3592, doi: [10.1093/mnras/stu1692](https://doi.org/10.1093/mnras/stu1692)
- Doyle, L., Cañas, C. I., Libby-Roberts, J. E., et al. 2024, arXiv e-prints, arXiv:2411.18567, doi: [10.48550/arXiv.2411.18567](https://doi.org/10.48550/arXiv.2411.18567)
- Eastman, J. 2017, EXOFASTv2: Generalized publication-quality exoplanet modeling code. <http://ascl.net/1710.003>
- Eastman, J. D., Rodriguez, J. E., Agol, E., et al. 2019, arXiv e-prints, arXiv:1907.09480. <https://arxiv.org/abs/1907.09480>
- ESA, ed. 1997, ESA Special Publication, Vol. 1200, The HIPPARCOS and TYCHO catalogues. Astrometric and photometric star catalogues derived from the ESA HIPPARCOS Space Astrometry Mission
- Espinosa-Retamal, J. I., Brahm, R., Petrovich, C., et al. 2023, ApJL, 958, L20, doi: [10.3847/2041-8213/ad096d](https://doi.org/10.3847/2041-8213/ad096d)

- Eversberg, T. 2016, PASP, 128, 115001, doi: [10.1088/1538-3873/128/969/115001](https://doi.org/10.1088/1538-3873/128/969/115001)
- Fabrycky, D., & Tremaine, S. 2007, ApJ, 669, 1298, doi: [10.1086/521702](https://doi.org/10.1086/521702)
- Ferreira dos Santos, T., Rice, M., Wang, X.-Y., & Wang, S. 2024, AJ, 168, 145, doi: [10.3847/1538-3881/ad6b7f](https://doi.org/10.3847/1538-3881/ad6b7f)
- Fitton, S., Tofflemire, B. M., & Kraus, A. L. 2022, Research Notes of the American Astronomical Society, 6, 18, doi: [10.3847/2515-5172/ac4bb7](https://doi.org/10.3847/2515-5172/ac4bb7)
- Fulton, B. J., Petigura, E. A., Blunt, S., & Sinukoff, E. 2018, PASP, 130, 044504, doi: [10.1088/1538-3873/aaaaaa8](https://doi.org/10.1088/1538-3873/aaaaaa8)
- Gaia Collaboration, Brown, A. G. A., Vallenari, A., et al. 2016, A&A, 595, A2, doi: [10.1051/0004-6361/201629512](https://doi.org/10.1051/0004-6361/201629512)
- . 2018, A&A, 616, A1, doi: [10.1051/0004-6361/201833051](https://doi.org/10.1051/0004-6361/201833051)
- Gaia Collaboration, Vallenari, A., Brown, A. G. A., et al. 2023, A&A, 674, A1, doi: [10.1051/0004-6361/202243940](https://doi.org/10.1051/0004-6361/202243940)
- Galvagni, M., & Mayer, L. 2014, MNRAS, 437, 2909, doi: [10.1093/mnras/stt2108](https://doi.org/10.1093/mnras/stt2108)
- Gan, T., Wang, S. X., Dai, F., et al. 2024, ApJL, 969, L24, doi: [10.3847/2041-8213/ad5967](https://doi.org/10.3847/2041-8213/ad5967)
- Garai, Z., Pribulla, T., Hambálek, L., et al. 2017, Astronomische Nachrichten, 338, 35, doi: [10.1002/asna.201613208](https://doi.org/10.1002/asna.201613208)
- Gelman, A., & Rubin, D. B. 1992, Statistical Science, 7, 457, doi: [10.1214/ss/1177011136](https://doi.org/10.1214/ss/1177011136)
- Giacalone, S., Dai, F., Zanazzi, J. J., et al. 2024, AJ, 168, 189, doi: [10.3847/1538-3881/ad785a](https://doi.org/10.3847/1538-3881/ad785a)
- Ginzburg, S., & Chiang, E. 2019, MNRAS, 487, 681, doi: [10.1093/mnras/stz1322](https://doi.org/10.1093/mnras/stz1322)
- Goldreich, P., Lithwick, Y., & Sari, R. 2004, ARA&A, 42, 549, doi: [10.1146/annurev.astro.42.053102.134004](https://doi.org/10.1146/annurev.astro.42.053102.134004)
- Goyal, A. V., Dai, F., & Wang, S. 2023
- Goyal, A. V., & Wang, S. 2022, ApJ, 933, 162, doi: [10.3847/1538-4357/ac7562](https://doi.org/10.3847/1538-4357/ac7562)
- Gray, R. O., & Corbally, C. J. 1994, AJ, 107, 742, doi: [10.1086/116893](https://doi.org/10.1086/116893)
- Gupta, A. F., Millholland, S. C., Im, H., et al. 2024, Nature, 632, 50, doi: [10.1038/s41586-024-07688-3](https://doi.org/10.1038/s41586-024-07688-3)
- Gustafsson, B., Edvardsson, B., Eriksson, K., et al. 2008, A&A, 486, 951, doi: [10.1051/0004-6361:200809724](https://doi.org/10.1051/0004-6361:200809724)
- Harris, C. R., Millman, K. J., van der Walt, S. J., et al. 2020, Nature, 585, 357
- Hébrard, G., Bouchy, F., Pont, F., et al. 2008, A&A, 488, 763, doi: [10.1051/0004-6361:200810056](https://doi.org/10.1051/0004-6361:200810056)
- Hébrard, G., Ehrenreich, D., Bouchy, F., et al. 2011, A&A, 527, L11, doi: [10.1051/0004-6361/201016331](https://doi.org/10.1051/0004-6361/201016331)
- Heiter, U., Lind, K., Bergemann, M., et al. 2021, A&A, 645, A106, doi: [10.1051/0004-6361/201936291](https://doi.org/10.1051/0004-6361/201936291)
- Hippke, M., David, T. J., Mulders, G. D., & Heller, R. 2019, AJ, 158, 143, doi: [10.3847/1538-3881/ab3984](https://doi.org/10.3847/1538-3881/ab3984)
- Hirano, T., Narita, N., Sato, B., et al. 2011a, PASJ, 63, L57, doi: [10.1093/pasj/63.6.L57](https://doi.org/10.1093/pasj/63.6.L57)
- Hirano, T., Suto, Y., Winn, J. N., et al. 2011b, ApJ, 742, 69, doi: [10.1088/0004-637X/742/2/69](https://doi.org/10.1088/0004-637X/742/2/69)
- Hixenbaugh, K., Wang, X.-Y., Rice, M., & Wang, S. 2023, ApJL, 949, L35, doi: [10.3847/2041-8213/acd6f5](https://doi.org/10.3847/2041-8213/acd6f5)
- Hjorth, M., Albrecht, S., Hirano, T., et al. 2021, Proceedings of the National Academy of Science, 118, e2017418118, doi: [10.1073/pnas.2017418118](https://doi.org/10.1073/pnas.2017418118)
- Holcomb, R. J., Robertson, P., Hartigan, P., Oelkers, R. J., & Robinson, C. 2022, ApJ, 936, 138, doi: [10.3847/1538-4357/ac8990](https://doi.org/10.3847/1538-4357/ac8990)
- Hu, Q., Rice, M., Wang, X.-Y., et al. 2024, arXiv e-prints, arXiv:2402.07346. <https://arxiv.org/abs/2402.07346>
- Hunter, J. D. 2007, Computing in science & engineering, 9, 90
- Ivshina, E. S., & Winn, J. N. 2022, ApJS, 259, 62, doi: [10.3847/1538-4365/ac545b](https://doi.org/10.3847/1538-4365/ac545b)
- Jenkins, J. M., Twicken, J. D., McCauliff, S., et al. 2016, in Society of Photo-Optical Instrumentation Engineers (SPIE) Conference Series, Vol. 9913, Software and Cyberinfrastructure for Astronomy IV, ed. G. Chiozzi & J. C. Guzman, 99133E, doi: [10.1117/12.2233418](https://doi.org/10.1117/12.2233418)
- Johns-Krull, C. M., McCullough, P. R., Burke, C. J., et al. 2008, ApJ, 677, 657, doi: [10.1086/528950](https://doi.org/10.1086/528950)
- Johnson, M. C., Cochran, W. D., Addison, B. C., Tinney, C. G., & Wright, D. J. 2017, AJ, 154, 137, doi: [10.3847/1538-3881/aa8462](https://doi.org/10.3847/1538-3881/aa8462)
- Kant, I. 1755, Allgemeine Naturgeschichte und Theorie des Himmels
- Khandelwal, A., Sharma, R., Chakraborty, A., et al. 2023, A&A, 672, L7, doi: [10.1051/0004-6361/202245608](https://doi.org/10.1051/0004-6361/202245608)
- Kipping, D. 2023, MNRAS, 523, 1182, doi: [10.1093/mnras/stad1492](https://doi.org/10.1093/mnras/stad1492)
- Kipping, D., & Wang, X.-Y. 2024, MNRAS, 532, 604, doi: [10.1093/mnras/stae1423](https://doi.org/10.1093/mnras/stae1423)
- Knudstrup, E., Albrecht, S. H., Winn, J. N., et al. 2024, A&A, 690, A379, doi: [10.1051/0004-6361/202450627](https://doi.org/10.1051/0004-6361/202450627)
- Knutson, H. A., Fulton, B. J., Montet, B. T., et al. 2014, ApJ, 785, 126, doi: [10.1088/0004-637X/785/2/126](https://doi.org/10.1088/0004-637X/785/2/126)
- Krolikowski, D. M., Kraus, A. L., & Rizzuto, A. C. 2021, AJ, 162, 110, doi: [10.3847/1538-3881/ac0632](https://doi.org/10.3847/1538-3881/ac0632)
- Li, G., & Winn, J. N. 2016, ApJ, 818, 5, doi: [10.3847/0004-637X/818/1/5](https://doi.org/10.3847/0004-637X/818/1/5)
- Lightkurve Collaboration, Cardoso, J. V. d. M., Hedges, C., et al. 2018, Lightkurve: Kepler and TESS time series analysis in Python, Astrophysics Source Code Library, record ascl:1812.013. <http://ascl.net/1812.013>
- Lindgren, L., Hernández, J., Bombrun, A., et al. 2018, A&A, 616, A2, doi: [10.1051/0004-6361/201832727](https://doi.org/10.1051/0004-6361/201832727)

- Lindegren, L., Klioner, S. A., Hernández, J., et al. 2021, *A&A*, 649, A2, doi: [10.1051/0004-6361/202039709](https://doi.org/10.1051/0004-6361/202039709)
- Lithwick, Y., & Wu, Y. 2014, Proceedings of the National Academy of Sciences, 111, 12610, doi: [10.1073/pnas.1308261110](https://doi.org/10.1073/pnas.1308261110)
- Lubin, J., Wang, X.-Y., Rice, M., et al. 2023, *ApJL*, 959, L5, doi: [10.3847/2041-8213/ad0fea](https://doi.org/10.3847/2041-8213/ad0fea)
- Mancini, L., Esposito, M., Covino, E., et al. 2015, *A&A*, 579, A136, doi: [10.1051/0004-6361/201526030](https://doi.org/10.1051/0004-6361/201526030)
- McKinney, W. 2010, in Proceedings of the 9th Python in Science Conference, Vol. 445, Austin, TX, 51–56
- McLaughlin, D. B. 1924, *ApJ*, 60, 22, doi: [10.1086/142826](https://doi.org/10.1086/142826)
- Millholland, S., Wang, S., & Laughlin, G. 2017, *ApJL*, 849, L33, doi: [10.3847/2041-8213/aa9714](https://doi.org/10.3847/2041-8213/aa9714)
- Moré, J. J. 2006, in Numerical analysis: proceedings of the biennial Conference held at Dundee, June 28–July 1, 1977, Springer, 105–116
- Nagasawa, M., & Ida, S. 2011, *ApJ*, 742, 72, doi: [10.1088/0004-637X/742/2/72](https://doi.org/10.1088/0004-637X/742/2/72)
- Nagasawa, M., Ida, S., & Bessho, T. 2008, *ApJ*, 678, 498, doi: [10.1086/529369](https://doi.org/10.1086/529369)
- Nelder, J. A., & Mead, R. 1965, *The Computer Journal*, 7, 308, doi: [10.1093/comjnl/7.4.308](https://doi.org/10.1093/comjnl/7.4.308)
- Ngo, H., Knutson, H. A., Hinkley, S., et al. 2015, *ApJ*, 800, 138, doi: [10.1088/0004-637X/800/2/138](https://doi.org/10.1088/0004-637X/800/2/138)
- Noguchi, K., Aoki, W., Kawanomoto, S., et al. 2002, *PASJ*, 54, 855, doi: [10.1093/pasj/54.6.855](https://doi.org/10.1093/pasj/54.6.855)
- Oliphant, T. E. 2006, A guide to NumPy, Vol. 1 (Trelgol Publishing USA)
- Perruchot, S., Kohler, D., Bouchy, F., et al. 2008, in Society of Photo-Optical Instrumentation Engineers (SPIE) Conference Series, Vol. 7014, Ground-based and Airborne Instrumentation for Astronomy II, ed. I. S. McLean & M. M. Casali, 70140J, doi: [10.1117/12.787379](https://doi.org/10.1117/12.787379)
- Radzom, B. T., Dong, J., Rice, M., et al. 2024, *AJ*, 168, 116, doi: [10.3847/1538-3881/ad61d8](https://doi.org/10.3847/1538-3881/ad61d8)
- Rasio, F. A., & Ford, E. B. 1996, *Science*, 274, 954, doi: [10.1126/science.274.5289.954](https://doi.org/10.1126/science.274.5289.954)
- Rice, M., Wang, S., Gerbig, K., et al. 2023a, *AJ*, 165, 65, doi: [10.3847/1538-3881/aca88e](https://doi.org/10.3847/1538-3881/aca88e)
- Rice, M., Wang, S., & Laughlin, G. 2022a, *ApJL*, 926, L17, doi: [10.3847/2041-8213/ac502d](https://doi.org/10.3847/2041-8213/ac502d)
- Rice, M., Wang, S., Howard, A. W., et al. 2021, *AJ*, 162, 182, doi: [10.3847/1538-3881/ac1f8f](https://doi.org/10.3847/1538-3881/ac1f8f)
- Rice, M., Wang, S., Wang, X.-Y., et al. 2022b, *AJ*, 164, 104, doi: [10.3847/1538-3881/ac8153](https://doi.org/10.3847/1538-3881/ac8153)
- Rice, M., Wang, X.-Y., Wang, S., et al. 2023b, *AJ*, 166, 266, doi: [10.3847/1538-3881/ad09de](https://doi.org/10.3847/1538-3881/ad09de)
- Ricker, G. R., Winn, J. N., Vanderspek, R., et al. 2015, *Journal of Astronomical Telescopes, Instruments, and Systems*, 1, 014003, doi: [10.1117/1.JATIS.1.1.014003](https://doi.org/10.1117/1.JATIS.1.1.014003)
- Rogers, T. M., Lin, D. N. C., & Lau, H. H. B. 2012, *ApJL*, 758, L6, doi: [10.1088/2041-8205/758/1/L6](https://doi.org/10.1088/2041-8205/758/1/L6)
- Rosenthal, L. J., Fulton, B. J., Hirsch, L. A., et al. 2021, *ApJS*, 255, 8, doi: [10.3847/1538-4365/abe23c](https://doi.org/10.3847/1538-4365/abe23c)
- Rossiter, R. A. 1924, *ApJ*, 60, 15, doi: [10.1086/142825](https://doi.org/10.1086/142825)
- Schlafly, E. F., & Finkbeiner, D. P. 2011, *ApJ*, 737, 103, doi: [10.1088/0004-637X/737/2/103](https://doi.org/10.1088/0004-637X/737/2/103)
- Schlaufman, K. C. 2010, *ApJ*, 719, 602, doi: [10.1088/0004-637X/719/1/602](https://doi.org/10.1088/0004-637X/719/1/602)
- Schmidt, S. P., Schlaufman, K. C., & Hamer, J. H. 2024, *AJ*, 168, 109, doi: [10.3847/1538-3881/ad5d76](https://doi.org/10.3847/1538-3881/ad5d76)
- Schmidt, S. P., Schlaufman, K. C., Ding, K., et al. 2023, *AJ*, 166, 225, doi: [10.3847/1538-3881/ad0135](https://doi.org/10.3847/1538-3881/ad0135)
- Scholz, F.-W., & Stephens, M. A. 1987, *Journal of the American Statistical Association*, 82, 918, <https://api.semanticscholar.org/CorpusID:38906795>
- Schwab, C., Rakich, A., Gong, Q., et al. 2016, in Society of Photo-Optical Instrumentation Engineers (SPIE) Conference Series, Vol. 9908, Ground-based and Airborne Instrumentation for Astronomy VI, ed. C. J. Evans, L. Simard, & H. Takami, 99087H, doi: [10.1117/12.2234411](https://doi.org/10.1117/12.2234411)
- Siverd, R. J., Beatty, T. G., Pepper, J., et al. 2012, *ApJ*, 761, 123, doi: [10.1088/0004-637X/761/2/123](https://doi.org/10.1088/0004-637X/761/2/123)
- Siverd, R. J., Collins, K. A., Zhou, G., et al. 2018, *AJ*, 155, 35, doi: [10.3847/1538-3881/aa9e4d](https://doi.org/10.3847/1538-3881/aa9e4d)
- Smith, A. M. S., Anderson, D. R., Collier Cameron, A., et al. 2012, *AJ*, 143, 81, doi: [10.1088/0004-6256/143/4/81](https://doi.org/10.1088/0004-6256/143/4/81)
- Southworth, J. 2011, *MNRAS*, 417, 2166, doi: [10.1111/j.1365-2966.2011.19399.x](https://doi.org/10.1111/j.1365-2966.2011.19399.x)
- Spalding, C., & Winn, J. N. 2022, *ApJ*, 927, 22, doi: [10.3847/1538-4357/ac4993](https://doi.org/10.3847/1538-4357/ac4993)
- Stassun, K. G., & Torres, G. 2018, *ApJ*, 862, 61, doi: [10.3847/1538-4357/aacafc](https://doi.org/10.3847/1538-4357/aacafc)
- Stefansson, G., Mahadevan, S., Petrovich, C., et al. 2022, *ApJL*, 931, L15, doi: [10.3847/2041-8213/ac6e3c](https://doi.org/10.3847/2041-8213/ac6e3c)
- Stumpe, M. C., Smith, J. C., Catanzarite, J. H., et al. 2014, *PASP*, 126, 100, doi: [10.1086/674989](https://doi.org/10.1086/674989)
- Stumpe, M. C., Smith, J. C., Van Cleve, J. E., et al. 2012, *PASP*, 124, 985, doi: [10.1086/667698](https://doi.org/10.1086/667698)
- Su, Y., & Lai, D. 2024, arXiv e-prints, arXiv:2411.08094, doi: [10.48550/arXiv.2411.08094](https://doi.org/10.48550/arXiv.2411.08094)
- Taylor, J., Claytor, Z. R., Huber, D., & van Saders, J. 2022, *ApJ*, 927, 31, doi: [10.3847/1538-4357/ac4bbc](https://doi.org/10.3847/1538-4357/ac4bbc)
- Temple, L. Y., Hellier, C., Albrow, M. D., et al. 2017, *MNRAS*, 471, 2743, doi: [10.1093/mnras/stx1729](https://doi.org/10.1093/mnras/stx1729)

- Ter Braak, C. J. F. 2006, Statistics and Computing, 16, 239, doi: [10.1007/s11222-006-8769-1](https://doi.org/10.1007/s11222-006-8769-1)
- Toci, C., Lodato, G., Christiaens, V., et al. 2020, MNRAS, 499, 2015, doi: [10.1093/mnras/staa2933](https://doi.org/10.1093/mnras/staa2933)
- Triaud, A. H. M. J. 2018, in Handbook of Exoplanets, ed. H. J. Deeg & J. A. Belmonte, 2, doi: [10.1007/978-3-319-55333-7_2](https://doi.org/10.1007/978-3-319-55333-7_2)
- Triaud, A. H. M. J., Queloz, D., Bouchy, F., et al. 2009, A&A, 506, 377, doi: [10.1051/0004-6361/200911897](https://doi.org/10.1051/0004-6361/200911897)
- Triaud, A. H. M. J., Collier Cameron, A., Queloz, D., et al. 2010, A&A, 524, A25, doi: [10.1051/0004-6361/201014525](https://doi.org/10.1051/0004-6361/201014525)
- Triaud, A. H. M. J., Hebb, L., Anderson, D. R., et al. 2013, A&A, 549, A18, doi: [10.1051/0004-6361/201219643](https://doi.org/10.1051/0004-6361/201219643)
- Tsantaki, M., Sousa, S. G., Santos, N. C., et al. 2014, A&A, 570, A80, doi: [10.1051/0004-6361/201424257](https://doi.org/10.1051/0004-6361/201424257)
- Tull, R. G. 1998, in Society of Photo-Optical Instrumentation Engineers (SPIE) Conference Series, Vol. 3355, Optical Astronomical Instrumentation, ed. S. D'Odorico, 387–398, doi: [10.1117/12.316774](https://doi.org/10.1117/12.316774)
- Tull, R. G., MacQueen, P. J., Sneden, C., & Lambert, D. L. 1995, PASP, 107, 251, doi: [10.1086/133548](https://doi.org/10.1086/133548)
- Valsecchi, F., & Rasio, F. A. 2014, ApJ, 786, 102, doi: [10.1088/0004-637X/786/2/102](https://doi.org/10.1088/0004-637X/786/2/102)
- Virtanen, P., Gommers, R., Oliphant, T. E., et al. 2020, Nature methods, 17, 261
- Vogt, S. S., Radovan, M., Kibrick, R., et al. 2014, PASP, 126, 359, doi: [10.1086/676120](https://doi.org/10.1086/676120)
- Walt, S. v. d., Colbert, S. C., & Varoquaux, G. 2011, Computing in Science & Engineering, 13, 22
- Wang, S. 2017, Research Notes of the American Astronomical Society, 1, 26, doi: [10.3847/2515-5172/aa9be5](https://doi.org/10.3847/2515-5172/aa9be5)
- Wang, S., Addison, B., Fischer, D. A., et al. 2018, AJ, 155, 70, doi: [10.3847/1538-3881/aaa2fb](https://doi.org/10.3847/1538-3881/aaa2fb)
- Wang, S., Winn, J. N., Addison, B. C., et al. 2021, AJ, 162, 50, doi: [10.3847/1538-3881/ac0626](https://doi.org/10.3847/1538-3881/ac0626)
- Wang, X.-Y., Rice, M., Wang, S., et al. 2022, ApJL, 926, L8, doi: [10.3847/2041-8213/ac4f44](https://doi.org/10.3847/2041-8213/ac4f44)
- . 2024, ApJL, 973, L21, doi: [10.3847/2041-8213/ad7469](https://doi.org/10.3847/2041-8213/ad7469)
- Weiss, L. M., Marcy, G. W., Petigura, E. A., et al. 2018, AJ, 155, 48, doi: [10.3847/1538-3881/aa9ff6](https://doi.org/10.3847/1538-3881/aa9ff6)
- Winn, J. N., Fabrycky, D., Albrecht, S., & Johnson, J. A. 2010, ApJL, 718, L145, doi: [10.1088/2041-8205/718/2/L145](https://doi.org/10.1088/2041-8205/718/2/L145)
- Winn, J. N., & Fabrycky, D. C. 2015, ARA&A, 53, 409, doi: [10.1146/annurev-astro-082214-122246](https://doi.org/10.1146/annurev-astro-082214-122246)
- Winn, J. N., Johnson, J. A., Fabrycky, D., et al. 2009, ApJ, 700, 302, doi: [10.1088/0004-637X/700/1/302](https://doi.org/10.1088/0004-637X/700/1/302)
- Wöllert, M., & Brandner, W. 2015, A&A, 579, A129, doi: [10.1051/0004-6361/201526525](https://doi.org/10.1051/0004-6361/201526525)
- Worku, K., Wang, S., Burt, J., et al. 2022, AJ, 163, 158, doi: [10.3847/1538-3881/ac4e1a](https://doi.org/10.3847/1538-3881/ac4e1a)
- Wright, J., Rice, M., Wang, X.-Y., Hixenbaugh, K., & Wang, S. 2023, arXiv e-prints, arXiv:2308.07532, doi: [10.48550/arXiv.2308.07532](https://doi.org/10.48550/arXiv.2308.07532)
- Wu, D.-H., Rice, M., & Wang, S. 2023, AJ, 165, 171, doi: [10.3847/1538-3881/acbf3f](https://doi.org/10.3847/1538-3881/acbf3f)
- Wu, Y., & Lithwick, Y. 2013, ApJ, 772, 74, doi: [10.1088/0004-637X/772/1/74](https://doi.org/10.1088/0004-637X/772/1/74)
- Wu, Y., & Murray, N. 2003, ApJ, 589, 605, doi: [10.1086/374598](https://doi.org/10.1086/374598)
- Xu, W., Jiang, Y.-F., Kunz, M. W., & Stone, J. M. 2024, arXiv e-prints, arXiv:2410.12042, doi: [10.48550/arXiv.2410.12042](https://doi.org/10.48550/arXiv.2410.12042)
- Xu, W., & Wang, S. 2024, ApJL, 962, L4, doi: [10.3847/2041-8213/ad1ee1](https://doi.org/10.3847/2041-8213/ad1ee1)
- Xue, Y., Suto, Y., Taruya, A., et al. 2014, ApJ, 784, 66, doi: [10.1088/0004-637X/784/1/66](https://doi.org/10.1088/0004-637X/784/1/66)
- Zanazzi, J. J., & Chiang, E. 2024, arXiv e-prints, arXiv:2410.10943, doi: [10.48550/arXiv.2410.10943](https://doi.org/10.48550/arXiv.2410.10943)
- Zanazzi, J. J., Dewberry, J., & Chiang, E. 2024, arXiv e-prints, arXiv:2403.05616, doi: [10.48550/arXiv.2403.05616](https://doi.org/10.48550/arXiv.2403.05616)
- Zhou, G., Rodriguez, J. E., Collins, K. A., et al. 2016, AJ, 152, 136, doi: [10.3847/0004-6256/152/5/136](https://doi.org/10.3847/0004-6256/152/5/136)
- Zhou, G., Rodriguez, J. E., Vanderburg, A., et al. 2018, AJ, 156, 93, doi: [10.3847/1538-3881/aad085](https://doi.org/10.3847/1538-3881/aad085)
- Zhou, G., Bakos, G. Á., Bayliss, D., et al. 2019a, AJ, 157, 31, doi: [10.3847/1538-3881/aaflbb](https://doi.org/10.3847/1538-3881/aaflbb)
- Zhou, G., Huang, C. X., Bakos, G. Á., et al. 2019b, AJ, 158, 141, doi: [10.3847/1538-3881/ab36b5](https://doi.org/10.3847/1538-3881/ab36b5)
- Zhu, Z., Hartmann, L., Nelson, R. P., & Gammie, C. F. 2012, ApJ, 746, 110, doi: [10.1088/0004-637X/746/1/110](https://doi.org/10.1088/0004-637X/746/1/110)